Article:
Cecchetto, M., Tregnaghi, M., Bottacin-Busolin, A. et al. (2018) Diffusive regimes of the motion of bed load particles in open channel flows at low transport stages. Water Resources Research, 54 (11). pp. 8674-8691. ISSN: 0043-1397

https://doi.org/10.1029/2018WR022885

AGU100 ADVANCING EARTH AND SPACE SCIENCE

Water Resources Research

RESEARCH ARTICLE
10.1029/2018WR022885

Key Points:
- The diffusive conceptual model for bed load transport is revised with two experimental data sets
- Subdiffusion is identified from long-term laboratory experiment with annular flume
- Ranges of motion and diffusive regimes are linked to Lagrangian time-dependent grain variables

Correspondence to:
M. Cecchetto,
mart.cecchetto@gmail.com

Citation:
Cecchetto, M., Tregnaghi, M., Bottacin-Busolin, A., Tait, S. J., Cotterle, L., & Marion, A. (2018). Diffusive regimes of the motion of bed load particles in open channel flows at low transport stages. *Water Resources Research*, *54*, 8674–8691. https://doi.org/10.1029/2018WR022885

Received 6 MAR 2018
Accepted 27 SEP 2018
Accepted article online 11 OCT 2018
Published online 5 NOV 2018

Diffusive Regimes of the Motion of Bed Load Particles in Open Channel Flows at Low Transport Stages

M. Cecchetto[1], M. Tregnaghi[2], A. Bottacin-Busolin[3], S. J. Tait[4], L. Cotterle[5], and A. Marion[2]

[1]WET Engineering srl, Castelfranco Veneto, Italy, [2]Department of Industrial Engineering, University of Padua, Padua, Italy, [3]School of Mechanical, Aerospace and Civil Engineering, The University of Manchester, Manchester, UK, [4]Department of Civil and Structural Engineering, The University of Sheffield, Sheffield, UK, [5]Mott MacDonald, Cambridge, UK

Abstract The stochasticity of fluid and sediment parameters has been identified as a source of diffusion, particularly anomalous diffusion at different temporal and spatial scales of bed load particle trajectories. Data from two sets of flume experiments are presented, one data set has gravel particle trajectories tracked over a limited area and was used in identifying the influence of different shear stress conditions on diffusive processes. A new experiment was performed using spherical particles moving as bed load in an annular flume in order to address concerns about censorship effects caused by the size of the detection window. An annular flume allowed collection of practically uncensored particle trajectories over longer time period than has been previously possible in the laboratory. Three diffusive regimes were observed at distinct stages of particle motion: (i) ballistic regime at the local range; (ii) Fickian diffusion at the intermediate range; (iii) subdiffusion at the global range. Characteristic time scales separate the regimes and correlate with the mean traveling and resting times of particles. Fickian diffusion in the intermediate range is first recognized as a result of the balance between intermittent weak transport and near-bed turbulence, as first predicted by Nikora et al. (2002, https://doi.org/10.1029/2001WR000513). In the global range, extreme values were observed in the distribution of particle resting times, suggesting that two types of distributions (related to surface motion and vertical mixing) were responsible for the subdiffusion at longer time scales. Diffusion was found to be anisotropic at all stages of particle motion.

1. Introduction

Particle dynamics in natural streams has seen growing interest throughout the twentieth century, initially driven by the need for solving engineering problems relevant to flood protection and river training (Vanoni, 1975; Yalin, 1972). More recently, the study of bed load dynamics has been sustained by the growing societal concerns over environmental problems related to both hydrogeological hazards and particulate-associated pollution (Marion et al., 2014). Assessing the fate of a cloud of sediments in rivers is crucial for determining, for example, the extent of a solid-phase contamination (Lajeunesse et al., 2013), the accumulation of cosmogenic radionuclides in sediment transport (Bradley et al., 2010), and, what is the subject of particular concern to date, the storage and transfer of microplastics in surface waters. In their study, Hurley et al. (2018) have shown that microplastic contamination in rivers is comparable to and, possibly, the source of ocean plastic content. Plastic fragments (attaining the size of 4–5 mm) move as discrete particles or they can be stored into the channel bed, where they pose a risk to the riverine ecosystem and from where they can be remobilized and transported downstream to estuarine areas.

Recently, bed load transport models have been proposed that invoke similar equations used to predict the advection and diffusion of solutes (e.g., Ganti et al., 2010; Lajeunesse et al., 2013), with the additional conceptual difficulty due to the heterogeneity that characterizes the bed compartment and the complexity of processes in sediment mechanics. These models are built upon the stochasticity of Lagrangian descriptors of bed load motion, for example, particle traveling and resting times, particle velocities and displacements (Nathan Bradley and Tucker, 2012). This motivated significant attention toward the topic of sediment diffusion following on the original impulse given by the conceptual model proposed by Nikora et al. (2002), so as to gain new evidence on the correlation between different stages of individual particle trajectories and ensemble diffusive regimes.

In the past decades, bed load particle motion has been either manually or automatically traced along a planar view of the bed in the longitudinal and lateral directions (e.g., Abbott & Francis, 1977; Bottacin-Busolin et al., 2008; Drake et al., 1987; Ferguson et al., 2002; Grass, 1970; Nikora et al., 2002; Nino & Garcia, 1996; Paintal,

1969; Tregnaghi, Bottacin-Busolin, Marion, et al., 2012; Tregnaghi, Bottacin-Busolin, Tait, et al., 2012), and on the vertical coordinate in terms of burial depth (Ferguson & Hoey, 2002; Haschenburger, 2011; Hassan et al., 1992; Hassan & Church, 1994; Wong et al., 2007). Interest in particle dynamics has also been caused by technological innovation in measurement systems allowing detailed observations not possible before. Increased image frequency acquisition, usually tens to hundreds of frames per second, enabled researchers to record individual grain locations and provided a reasonable Lagrangian description of particle trajectories. Results revealed that bed load displacements can be well represented by stochastic variables (e.g., Campagnol et al., 2013; Lajeunesse et al., 2010; Roseberry et al., 2012). This behavior derives from the combined effects of near-bed turbulent flows and local heterogeneities of river bed surfaces as the physical sources of mass diffusion (Drake et al., 1987; Ganti et al., 2010; Hassan et al., 2013; Martin et al., 2012; Nikora et al., 2002; Wong et al., 2007).

Diffusion can be estimated from the ensemble variation in time of particle positions over a bed surface. However, in riverine environments the observation of particle displacements is limited by the capability of field survey techniques, which achieve relatively low recovery rates of tracer grains. Despite the more recent technological improvement that led to recovery rates of 95% (Bradley, 2017), tracer particle locations are surveyed over time scales of days, months, or even years (Ferguson & Hoey, 2002; Haschenburger, 2011) or immediately after intense flow events (Bradley et al., 2010; Ferguson & Wathen, 1998; Hassan et al., 2013); thus, only information on the cumulative distance traveled by a particle between consecutive observations is available. Field studies inherently lack of a continuous record of particle locations that is needed to evaluate the diffusive character at different stages of particle motion. Even if this has now been made possible at the laboratory scale, the areal extent of the observed bed surface is usually restrained to a scale of tens of centimeters due to equipment constraints for image acquisition (Heays et al., 2014; Lajeunesse et al., 2010; Nikora et al., 2002; Tregnaghi, Bottacin-Busolin, Tait, et al., 2012), thus the motions of particles that enter or leave the video sampling area are spatially censored (Fan et al., 2017; Fathel et al., 2015). Accurate reconstruction of particle trajectories is dependent on the frequency of the image acquisition, as a higher frame rate can support more accurate measurement of grain trajectories. However, processing a large number of frames over long experiments is time and resource consuming. These inherent difficulties in performing experiments with tracers have produced cascading effects on the ability to gain in-depth knowledge of bed load dynamics at the grain scale (Furbish, Roseberry, et al., 2012) and thus limit our comprehension of the diffusive behavior of particle motion (Martin et al., 2012).

In spite of its theoretical and practical implications, sediment diffusion is probably one of the least understood mass transport mechanisms, and even fundamental questions still await clarification. There are several reasons why the movement of bed load particles rolling or saltating on the river bed surface should not conform with the assumption of *normal* diffusion. If normal diffusion is assumed to hold, particles are expected to move continuously, in contrast, bed load particles are observed to alternate quick movements to longer resting periods. Bouchaud and Georges (1990) described this process as "diffusion among traps", where long-range correlations in the flow turbulence have been claimed to occur (Nikora et al., 2002), and heavy-tailed distributions of particle motion arise from the effect of local bed heterogeneities on entrainment and distrainment of particles (Martin et al., 2012). In turn, bed load motion is likely to follow an *anomalous* diffusion process, that is, ballistic, subdiffusive, or superdiffusive, as predicted in the conceptual model first presented by Nikora et al. (2001, 2002). These authors associated the temporal and spatial scales of bed load motion with relevant diffusive regimes and identified three well-distinguished scale-dependent ranges: (a) the *local range* (ballistic diffusion), which corresponds to particle trajectories between two consecutive collisions with the bed; (b) the *intermediate range*, which refers to particle displacements between two subsequent periods of rest (normal or anomalous diffusion); and (c) the *global range* (subdiffusion), where the particle trajectories consist of many intermediate steps. The type of diffusion is determined by time-dependent power laws of the central moments of the particle coordinates:

$$\begin{aligned} \overline{X'^q} &= \left(\overline{X(t) - \overline{X}(t)}\right)^q \propto t^{q\gamma_x} \\ \overline{Y'^q} &= \left(\overline{Y(t) - \overline{Y}(t)}\right)^q \propto t^{q\gamma_y} \end{aligned} \tag{1}$$

where $X(t)$, $Y(t)$ denote longitudinal and transverse particle coordinates, q is the moment order, overbar denotes ensemble averaging, and t indicates the elapsed time. For the second-order moments, $q = 2$,

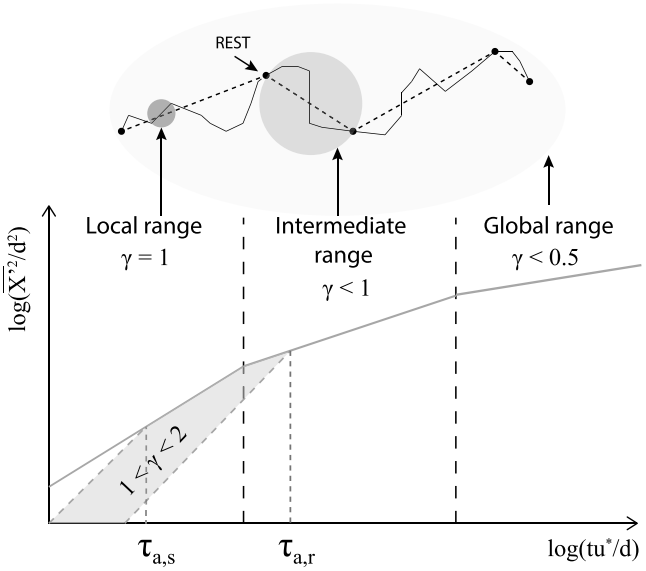

Figure 1. Conceptual model of longitudinal particles diffusion. Characteristic times $\tau_{a,s}$ and $\tau_{a,r}$ indicate the duration of the acceleration for saltating and rolling particles, respectively. After Campagnol et al. (2015).

the type of diffusive regime is specified by the scaling coefficients γ_x and γ_y: (i) anomalous diffusion ($\gamma \neq 0.5$), being it ballistic ($\gamma = 1$), superdiffusive ($\gamma > 0.5$), or subdiffusive ($\gamma < 0.5$); and (ii) normal diffusion ($\gamma = 0.5$). Following Nikora et al. (2002), $\overline{X'^2}$ and $\overline{Y'^2}$ are expressed as a function of the shear velocity, the particle diameter d and the elapsed time t (= total time spent in motion or at rest from the beginning of the observation period):

$$\frac{\overline{X'^2}}{\overline{d^2}}, \frac{\overline{Y'^2}}{\overline{d^2}} \propto \left(\frac{tu^*}{d}\right)^{2\gamma} \tag{2}$$

equation (2) has been applied in several studies, all confirming the anomalous nature of bed load transport, but with scaling diffusive coefficients falling within a relatively wide range (Bialik et al., 2012, 2015; Campagnol et al., 2015; Furbish, Ball, & Schmeeckle, 2012; Martin et al., 2012). According to Fan et al. (2017), discrepancies may emerge as a consequence of selected experimental conditions, with major inconsistency resulting from defining the accurate boundaries of the local range (because of the high frame rate required) and of the global range (because of the large temporal and spatial observation windows required; Bialik & Karpiński, 2018). Campagnol et al. (2015) revisited the original theoretical framework to attempt to explain evidence that superballistic diffusion ($1 < \gamma < 2$) was observed in the local range during the early unsteady stage of particle entrainment (the so called *near-field subrange* influenced by particle acceleration as reported in Bialik et al., 2015). Their revised model is presented in Figure 1 for the longitudinal diffusive process. Due to scarcity of experimental data, particularly in the range of $3.5 \cdot 10^3 < tu^*/d < 3.0 \cdot 10^6$ (Bialik et al., 2012, 2015), uncertainty still affects the identification of accurate temporal boundaries of different ranges and the correct assessment of diffusive regimes.

In this study the existing conceptual model is critically revised for both the two planar components of sediment motion. Diffusion of bed load particles is examined accounting for two different starting points of individual trajectories (namely, diffusion from entrainment and diffusion from randomly selected points). The aim is to discriminate the effects on the diffusive regime of inertial and frictional forces, respectively, which represent key drivers acting at different temporal and spatial scales of grain motion. To do this, a first set of short-term time series data was used as part of an experiment designed to study the correlation between grain-scale turbulence in open-channel flows and the transport of natural gravel material at weak transport stages (Cecchetto et al., 2016; Tregnaghi, Bottacin-Busolin, Tait, et al., 2012). A new experimental data set is then presented in this study that was obtained from longer observations carried out in an annular flume. This enabled the acquisition of relatively long time series compared with typical laboratory-scale experiments. A population sample of practically uncensored particles trajectories ensured that the global range was well represented in the experiment, and that censorship effects on the identification of diffusion regimes were critically addressed.

The paper is structured as follows: section 2 presents the experimental campaigns, including a detailed description of the image acquisition system used with the annular flume. Section 3 specifies the methodology applied in the data analysis for the reconstruction of particle trajectories. Results on the diffusive nature of particles along the longitudinal and transverse directions are presented in section 4. In section 5 the conceptual model of Nikora et al. (2002) is revised by linking the observed ranges of motion to well defined time-dependent scales of bed load diffusion accounting for particle (1) acceleration time, (2) traveling time, and (3) resting time.

2. Experimental Apparatus

Experiments were performed in two different types of laboratory flume that provided complimentary data sets of bed load particle trajectories. In the first series of tests sediment motion was observed over a natural gravel bed placed in a straight flume, where individual grains were traced over a 220-mm-long, 80-mm-wide

Table 1
Experimental Parameters: Shear Velocity u, Shields Parameter τ^* and Critical Shields Ratio τ^*/τ^*_{cr}, With τ^*_{cr} Following the Expression Reported in Van Rijn"s (1984)*

TEST	u^* (m/s)	τ^* (–)	τ^*/τ^*_{cr} (–)	# of trajectories from entrainment	# of trajectories from random point
B1	0.070	0.061	1.15	150	199
B2	0.074	0.068	1.28	342	512
B3	0.080	0.080	1.51	184	245
B4	0.081	0.083	1.57	167	241
B5	0.083	0.086	1.62	270	431
B6	0.085	0.090	1.70	123	241
S1	0.046	0.055	1.12	242	243

Note. u^* = shear velocity; τ^* = shields parameter; and τ^*/τ^*_{cr} = critical shields ratio, with τ^*_{cr} following the expression reported in Van Rijn's (1984). The total number of grain trajectories in each test is reported from entrainment and randomly selected points. Tests B1 to B6 were carried out in the straight flume, while test S1 in the annular flume.

observation area of the bed surface for short-duration runs (~2 min). Since these experiments were originally planned with a stereoscopic two-camera Particle Image Velocimetry system, the size of the area and the duration of the runs were selected as a compromise between attaining a sediment-size spatial image resolution and detecting a statistically significant number of grain entrainments (i.e., >100). The second data set of bed load particle trajectories was obtained with continuous video recording for prolonged observation periods (up to a maximum of 6 hr) in an annular flume with glass spheres forming the bed material. This enabled Lagrangian measurements of sediment motion with no spatial limitation in the streamwise extent of the observation window and with practically no mass loss during the experiment.

The first series of experiments was carried out in a 12-m-long, 0.46-m-wide, straight tilting flume. The channel bed was filled with natural gravel-sized grains with lognormal grain size distribution having mean diameter d_{50} = 5.0 mm and standard deviation σ_g = 1.3 mm. The density of the gravel was ρ_s = 2,650 kg/m^3. The material was arranged to form a uniform, well mixed, 60-mm-deep layer of sediment and scrapped flat at the beginning of each test. The initial 1.5-m-long inlet reach contained static gravel to ensure the consistent development of a stable turbulent boundary layer. For each test steady, uniform flow conditions were attained and no significant spatial pattern nor bed forms were observed over the sediment bed for the duration of the experiment. The flume was equipped with a video camera capturing images of the bed surface at a frequency of 45 Hz, with resolution 7.5 pixel/mm. The camera was placed vertically over the selected observation area (220-mm-long, 80-mm-wide), and located along the centerline of the flume bed 6.70 m downstream from the inlet. This enabled a population sample of ~800–900 individual particles composing the surface layer of the investigation area to be observed at each recording time. In total 12 tests were carried out with increasing bed shear stress and constant water depth h_u = 100 mm (more details are in Tregnaghi, Tregnaghi, Bottacin-Busolin, Tait, et al., 2012 and Cecchetto et al., 2016). Following Schmeeckle and Nelson (2003), in the selected tests B1 to B6 (Table 1) the ratio between the Shields parameter and the critical Shields parameter, τ^*/τ^*_{cr}, ranged from 1.15 (low transport stage) to 1.70 (moderate transport stage), where τ^*_{cr} = 0.053 is calculated with the reformulated Shields' expression reported in van Rijn's (1984). These conditions allowed for the clear identification of a number of individual grain entrainments ranging from ~120 to 350 and a total number of particle trajectories ranging from ~200 to 500 (see Table 1) over the area of the bed surface recorded with the image acquisition system, providing values of sediment discharge per unit width ranging in 2–8 g/sm. In this study 6,000 frames (about 2 min of observations) were analyzed for each test.

The second experiment was performed in an annular flume (hereafter denoted as S1). This flume setup simulates a *long* river reach, where the bed material and the fluid are not externally recirculated, and a uniform shear stress is applied to the bed. The flow is generated by the movement of the flume boundaries, that is, the lower plate integral with the walls and the upper lid in direct contact with the water surface. This system generates steady equilibrium conditions and enables long duration experiments (e.g., Booij, 1994; Gharabaghi et al., 2007; James et al., 1996; Partheniades et al., 1966). A sketch of the flume is presented in Figure 2. The external and internal diameters of the flume are, respectively, 2.20 m and 1.80 m. The

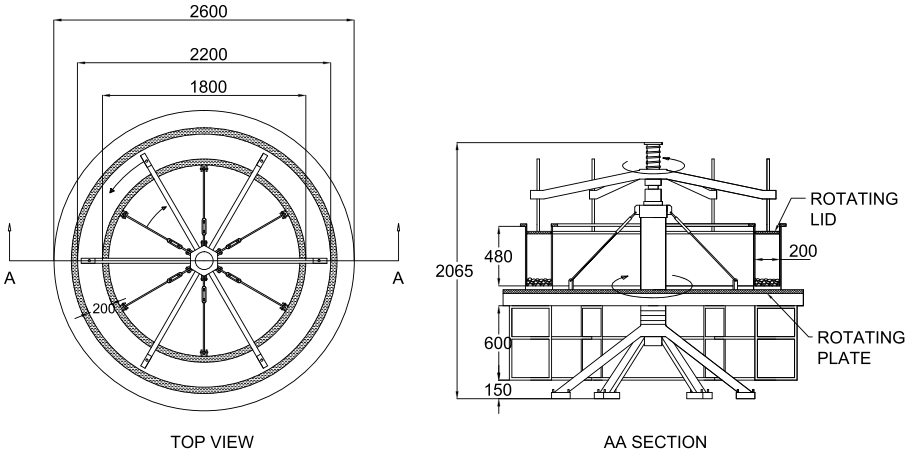

Figure 2. Top view of and vertical cross section (AA) of the annular flume. All dimensions in millimeters.

rectangular cross section is b = 0.20-m-wide and the maximum available height is H = 0.48 m. The side walls and the bottom plate are made of transparent Perspex to allow for continuous particle visualization during the experiment. The lid is made of dark gray polyvinyl chloride and can be manually lowered or lifted to set the desired water depth.

The generation of secondary currents due to the curvature of the flume was minimized by setting the rotational velocities of the top lid, ω_t, and of the bottom, ω_b, to a fixed ratio (Booij, 1994; Partheniades et al., 1966). Calibrating the *optimal ratio* ω_t/ω_b generated counteracting secondary currents, which ensured quasi-two-dimensional flow conditions were attained. The determination of the optimal value of ω_t/ω_b was achieved by direct observation of displacements of plastic beads with density slightly higher than water density (Partheniades et al., 1966) and size smaller than the boundary layer structure of the bottom. The intensity of secondary currents was assumed negligible when the beads were observed to move steadily along the centerline of the channel bottom. With these conditions attained, uniform distributions of tangential velocity and near-bed stress were reasonably assumed to hold (Booij, 1994; Partheniades et al., 1966).

Preliminary tests were performed to calibrate the optimal ratio for different water depths (Figure 3a). The operative water depth H was set equal to 0.30 m; as for this value secondary current effects associated to either shallow or large flow depths were observed to be negligible or almost absent (Booij, 1994). The same

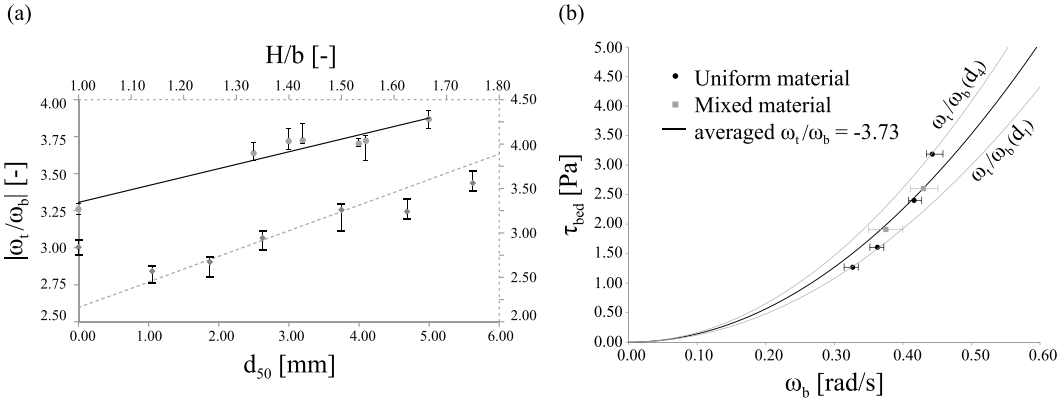

Figure 3. (a) Magnitude of optimal rotational velocity ratio versus bed roughness d_{50} (solid lines and axes), and versus water depth-to-width ratio (dashed line and axes). Both left and right vertical axes indicate the optimal ratio. (b) Bed shear stress versus bottom rotational velocity. The black line is obtained for $\omega_t/\omega_b = -3.73$. All data falls within the two upper and lower boundaries obtained, respectively, for the uniformly sized mixtures d_4 = 5 mm and d_1 = 2.5 mm (gray lines).

procedure was used to correlate the optimal ratio with the bed roughness, which was assumed to correlate well with the mean size, d_{50}, of the relatively uniform bed material (Figure 3a) and to test the relationship between the bed shear stress and rotational velocities against the theoretical formulation presented by Booij (1994; Figure 3b). Following Booij's methodology, which implicitly accounted for the correction due to the effects of the later walls, the predicted increase of the bed shear stress with the rotating velocity was confirmed for six different sizes of bed particles, which consistently supported validation of the calibration procedure. Tests were carried out by (i) minimizing secondary current effects through the adjustment of top-to-bottom ratio of the rotational velocities; and afterward (ii) attaining the threshold of particle motion by direct visual inspection, with multiple assessments performed by different observers (which is graphically represented by error bars in figures). All sizes of bed material consisted of transparent borosilicate glass spheres with density ρ_s = 2,230 kg/m^3. Four uniform size classes were composed of similar spheres manufactured with approximately 90% accuracy, that is, d_1 = 2.5 ± 0.3 mm, d_2 = 3.0 ± 0.3 mm, d_3 = 4.0 ± 0.3 mm, d_4 = 5.0 ± 0.3, and two uniform mixtures were created out of these four classes. The first mixture consisted of d_2, d_3, and d_4 sphere sizes, with mean diameter $d_{50,1}$ = 4.1 mm and standard deviation σ_g = 1.33. A finer mixture was composed of d_1, d_2, and d_3 sphere sizes, resulting in $d_{50,2}$ = 3.2 mm and standard deviation σ_g = 1.37. The increase of the shear stress as a function of the bottom velocity, originally predicted for uniform material by Booij (1994), was confirmed also in the tests with mixed material (Figure 3b).

The image acquisition system is shown in Figure 4a. Six GoPro cameras were fixed so that they moved with the bottom plate of the flume. Six vertical bars held the top-view cameras providing a sufficient image overlap from adjacent cameras (Figure 4a), and the cameras were tilted at 50° with respect to the vertical plane at a height of 500 mm. The cameras recorded at 30-Hz-frequency for up to 7 hr with a resolution of 2 pixel/mm. Cameras were remotely controlled and synchronized with a light pulse at the beginning of the test.

A radial-shaped checkerboard was created to transform the distorted image of the circular channel into one representing a continuous straight bed. The radial component r was transformed into the transverse coordinate y, whereas the angular component θ was replaced by the longitudinal coordinate x (Figure 4b). Due to the relatively small flume curvature, that is, b/R = 0.20 with R = 1 m the flume radius, the arc lengths were marginally affected by distortion effects as illustrated in Figure 4b. To obtain a regular square grid, the algorithm preserved the original crosswise dimension, stretched the inner checkers, and compressed the outer squares. The measured distance traveled by bed load particles was then corrected depending on the particle crosswise coordinates to counteract the effects of the stretch-compression algorithm. This correction was applied to each recorded position of the particle trajectory (sampling rate = 0.033 s), so that the location was continuously adjusted along the entire path traveled by each particle.

After completion of the calibration procedure a test was carried out to observe long-term diffusion of bed load sediment transport by recording the movement of a small group of tracer particles. The bed material consisted of a scrapped flat 35-mm-thick deposit (corresponding approximately to 10 d_{50}), and it was composed of mixed size transparent borosilicate glass spheres distributed in particle size according to the fine mixture ($d_{50,2}$ = 3.2 mm, σ_g = 1.37 mm). A group of borosilicate black spheres with diameter d = 4 mm were used as tracing particles. The tracer size was comparable to the size d_3 of the largest particles in the fine mixture. The black spheres replaced the same size material according to the mixture proportions, that is, 25% in weight, in a surficial strip 10-mm thick (see Figure 4c). The applied shear velocity resulted in the Shields parameter τ^* = 0.055 and excess shear stress τ^*/τ^*_{cr} = 1.13, where τ^*_{cr} = 0.049 (van Rijn, 1984). The experiment was run for 6 hr during which the motion of the tracers was continuously recorded. The total duration of the experiment was imposed by the maximum recording capacity of the GoPro cameras. This temporal scale corresponds approximately to $tu^*/d = 0.2–0.3 \cdot 10^5$, which ensured collection of data falling within the global range (e.g., Bialik & Karpiński, 2018), and it extended well beyond the duration used in similar studies on bed load sediment transport (e.g.: Campagnol et al., 2013; Lajeunesse et al., 2010; Nikora et al., 2002; Roseberry et al., 2012).

The trajectories of the traced black spheres from test S1 were first analyzed to confirm no appreciable secondary current effects were observed. These are expected to be visible in the statistics of the transverse component of the particle step. Figure 4d shows that the crosswise steps symmetrically distribute around zero with average value of −0.22 mm, corresponding to 5% of the tracing sphere diameter, which confirms transverse spatially uniform flow conditions were attained.

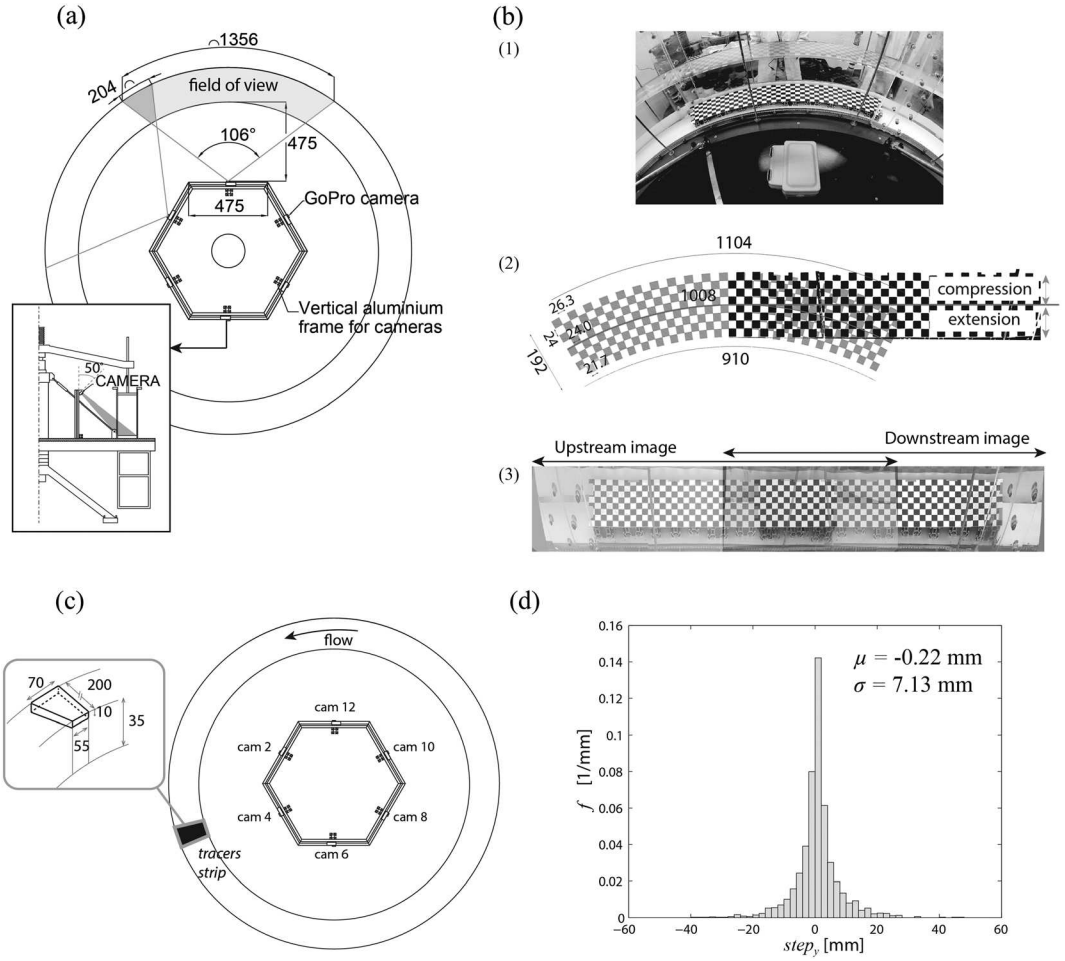

Figure 4. (a) Top cross-sectional view of the flume with camera positions and field of view. (b) Image sample taken from one camera overlooking the submerged checkerboard (1); actual checkerboard size (in light gray) with superimposed checkerboard transformation (2); postcalibration image sample obtained with two overlapping frames from adjacent cameras (3). (c) Schematic representation of the experimental setup of test S1 with initial locations of the tracer particle strip. (d) Frequency distribution of the tracers' crosswise step length. All dimensions in millimeters.

3. Methodology: Reconstruction of Particle Trajectories

Diffusion parameters were estimated from the variation in time of particle coordinates. A common reference system was established for all the moving grains. For each test recorded grain locations, $X_i(t)^*$ and $Y_i(t)^*$, were translated to the same origin point according to the transformation $X_i(t) = X_i(t)^* - X_i(t_0)^*$ and $Y_i(t) = Y_i(t)^* - Y_i(t_0)^*$, where $X_i(t_0)^*$ and $Y_i(t_0)^*$ are the first recorded streamwise and crosswise positions, respectively, of the ith grain in correspondence of particle motion state at t_0.

In the next sections, the diffusive scaling coefficients were obtained for trajectories originating, respectively, from (a) an entrainment event; and (b) a random moving state along the particle path. Accounting for different motion states at t_0 (denoting the starting time of the trajectory) supports the identification of the effects on the diffusive regime of inertial and frictional forces, respectively, which act at different stages of particle motion (Bialik et al., 2012, 2015; Campagnol et al., 2015). The type of diffusive processes is thus dependent on the motion state occupied by a particle at t_0, namely, an entrainment event or a moving state. In the latter, the origin of the ensemble trajectories, $X_i(t_0)^*$, is defined by the position of a particle during its motion. This either corresponds to the accelerating or decelerating phases, respectively, of an entrainment or distrainment event (Campagnol et al., 2015) or can be identified as the quasi-steady stage of motion where the particle has no memory of earlier phases (Bialik et al., 2015). In turn, this approach accounts for

the diffusive behavior of the ensemble bed load flux, and the relevant analysis enables identification of the diffusive regime in the local range, as entrainments will no longer significantly contribute to the diffusion process.

A third approach based on collision points of a particle with the bed surface as the origin of its trajectory can be applied to determine the diffusive behavior in the local range at or just after the instant of collision. However, both experimental setups described in this study had no camera focused on a vertical plane, thus collision events could not be assessed accurately.

In all the experiments (straight and annular flume) the reconstruction of particle trajectories required the acquisition of the position of moving grains at consecutive times at an appropriate sampling rate. Particle positions were extracted from the bed images using a manual tracking following the method developed by Bottacin-Busolin et al. (2008). Each grain was classified according to its state, depending on whether it was starting to move (*start*), moving (*move*), or stopping (*stop*). This information, along with the centroid locations of the detected particles, was stored in a database and allowed the later reconstruction of grain trajectories.

The two types of experimental setups mainly differ in that the identification and selection of grains being tracked consisted either of the whole population of particles in motion (straight flume) or of a given subset established a priori by the observer (black spheres for the annular experiment). The trajectory traveled by each individual grain was reconstructed based on the following criteria: (i) definition of a temporal threshold for the duration of a competent resting time; and (ii) definition of a spatial motion threshold to discard very small displacements.

In order to specify the temporal criterion, from the observation of hundreds of grain movements, it became apparent that the identification of particle resting times was dependent on the subjective judgment of an observer. A grain during its motion was observed to halt in a resting state for a few frames ($<$0.1 s) and then start moving again along its travel path. A minimum resting time t_{min} = 0.10 s was selected based on previous findings by Nelson et al. (1995), reporting high correlations between entrainment events and near-bed streamwise velocities measured approximately up to 0.10 s before transport occurred in weakly mobile beds. Similar observations (from tests B1 to B6 in this study) were later confirmed by Cecchetto et al. (2016), who found that most particles were entrained by bursting events with duration of 0.05 to 0.1 s This value provides mean duration of normalized bursting events, $T\overline{u}_{max}/H$ (with $T = t_{min}$ the duration of the bursting event, $\overline{u}_{max}$ the surface water velocity, and H the water depth), in the range 1.0 to 3.0, in agreement with earlier observations by Nikora and Goring (2000), Nezu and Nakagawa (1993), and Dey et al. (2011).

Following the observations of Campagnol et al. (2013), the spatial threshold was identified by what is referred to as particle vibrations, which were discarded from the population of particles in motion in this study. If a grain moved along the longitudinal coordinate, from entrainment to rest, a distance smaller than its diameter, such a short displacement was neglected, since it was considered an adjustment toward a stable position rather than an active motion. This physical interpretation stems from assuming a grain re-adjusting its pocket position on the bed as the latter is subject to different forces compared to a grain moving through the fluid. The former is mainly affected by frictional forces, the latter is mostly influenced by fluid drag (Cecchetto et al., 2016).

From an operational point of view, a further element that poses a key issue is the window effect (or censorship), that is the systematic error in which those particles that potentially make a major contribution to the diffusion are omitted (Bialik & Karpiński, 2018). For the first set of experiments having an observation area with assigned physical boundaries, only uncensored trajectories were measured, while grain paths with a starting position from outside and exiting the investigated area (i.e., spatially censored) were neglected. In the initial diffusion stages boundary effects are negligible, but they become relevant in the evaluation of the global range. For the tests in the straight flume no global trajectories consisting of more than five intermediate steps were observed, with a majority of trajectories consisting of one to two intermediate steps. In the annular flume, a particle could potentially be followed from its first entrainment to the end of the experiment. However, tracking was performed only with images collected from one camera, specifically from camera 4 located above the tracer strip. The 1-m-long area covered by the camera lens was sufficient to fully describe the trajectories of all particles, so that no observations were made of displacements with missing simultaneously *start* and *stop* positions. A fraction of particles were observed leaving to the adjacent zone

or entering from an upstream location; however, (a) their relative occurrence was significantly lower compared to the tests in the straight flume; (b) before leaving or after entering the image boundaries they moved over a 1-m-long area performing on average nine intermediate steps.

In test S1 the full recording session (approx. 6 hr corresponding to 648,000 frames) was split into 10 subsessions comprising 12,000 frames each (~400 s). Tracer spheres were followed over the entire duration of each subsession, and the resulting subdata sets were merged together to form a well-populated database of particle trajectories. Closer inspection of particle trajectories from individual subsessions confirmed the assumption of statistical stationarity of the process over the 6 hr. The subsession time-averaged first- and second-order moments (mean and standard deviation) of sampled streamwise and crosswise steps traveled by the tracers were observed to fluctuate around the full-run time-averaged values with no significant temporal trend. This also confirms that secondary current effects were negligible or absent, and that the stretch-compression algorithm was applied consistently throughout the whole length of the annular flume. The total number of sampled trajectories for the tests in the straight and annular flumes, respectively, is reported in Table 1.

4. Results

4.1. Longitudinal Diffusive Regimes

Results of the longitudinal diffusive trends are shown in Figure 5. Accounting for the initiation of motion (entrainment events) as the starting point of grain trajectories, three distinguished regions can be clearly identified that are denoted by constant scaling coefficients (Figure 5a). The region in the initial stage of particle motion is apparently governed by ballistic diffusion, with γ_x attaining values close to 1. The solid line corresponding to $\gamma_x = 1$ in Figure 5a provides a qualitative comparison between the theoretical ballistic diffusive regime and observed trend of the experimental data.

The apparent ballistic diffusion in Figure 5a is contested by a closer inspection of data provided by Figure 5b, where short-term fluctuations of γ_x were filtered by using a moving average with sample window = 3 data points in the ballistic diffusion region, and averaged values of γ_x were plotted against tu^*/d. For tests in the straight flume (solid lines), γ_x attains values up to 1.5 (test B1) for $tu^*/d \leq 1$ (except for tests B2 and B5, where $\gamma_x \approx 1.0$), then becomes equal to 1.0 for $tu^*/d \approx 3.0$. However, the initial diffusive behavior for test S1 (cross marks in Figure 5a and dashed line in Figure 5b) shows larger values of γ_x, exhibiting a peak of up to 1.8 in the very early stage of motion and a rapid decrease to the ballistic zone for larger times ($tu^*/d > 5$).

After the superballistic region, a transition phase characterized by a rapidly decreasing diffusive coefficient takes place till $tu^*/d = 10$. A second region of constant diffusive coefficient develops starting from $tu^*/d = 10$ (Figure 5a). In this region diffusion becomes normal, exhibiting constant $\gamma_x = 0.5$ for $tu^*/d < 100$. This is apparent for the data series S1 (annular flume), whereas $\overline{X'^2}$ increases at a lower rate for the B tests ($\gamma_x = 0.10$) compared to the population of uncensored particle trajectories. For $tu^*/d > 100$ a subdiffusive regime is observed to occur with mean diffusive coefficient approaching $\gamma_x = 0.30$ (solid line in Figure 5a).

Following Nikora et al. (2002), $X(t)$ was reconstructed starting from a random coordinate along the particle path. The population sample consisted of particles with fully observed paths within the area, including those particles that entered the area while in motion. For the latter, $X_i(t_0)^*$ corresponded to the first detected position when the grain entered the area. The variation in time of $\overline{X'^2}$ presents three regions identified by constant diffusive scaling coefficients (Figure 5c**)**. The first regime takes place at the beginning of the trajectories, covering the sequence of collisions with the bed before a final stop is achieved. Data from both B tests and test S1 exhibit a diffusive coefficient $\gamma_x = 1.0$, as represented by the solid line. The ballistic regime is confirmed from observations of the local variation of γ_x with no evidence of the initial acceleration phase. When the ensemble flux of particles is observed while in motion, disregarding the contribution of entrainment and distrainment events, the local range closely approaches a ballistic diffusive process (i.e., $\gamma_x = 1.0$), regardless of the stage of the transport conditions. For $3 < tu^*/d < 10$ particle motion follows a region of transition, which starts later for test S1 ($tu^*/d \approx 5$). As a consequence γ_x in this range is not uniquely identified by a single value, but it rather decreases smoothly to a Fickian diffusive behavior that continues invariant for $10 < tu^*/d < 100$. At the end of the region with constant $\gamma_x = 0.50$, the process is observed to follow a subdiffusion regime, as

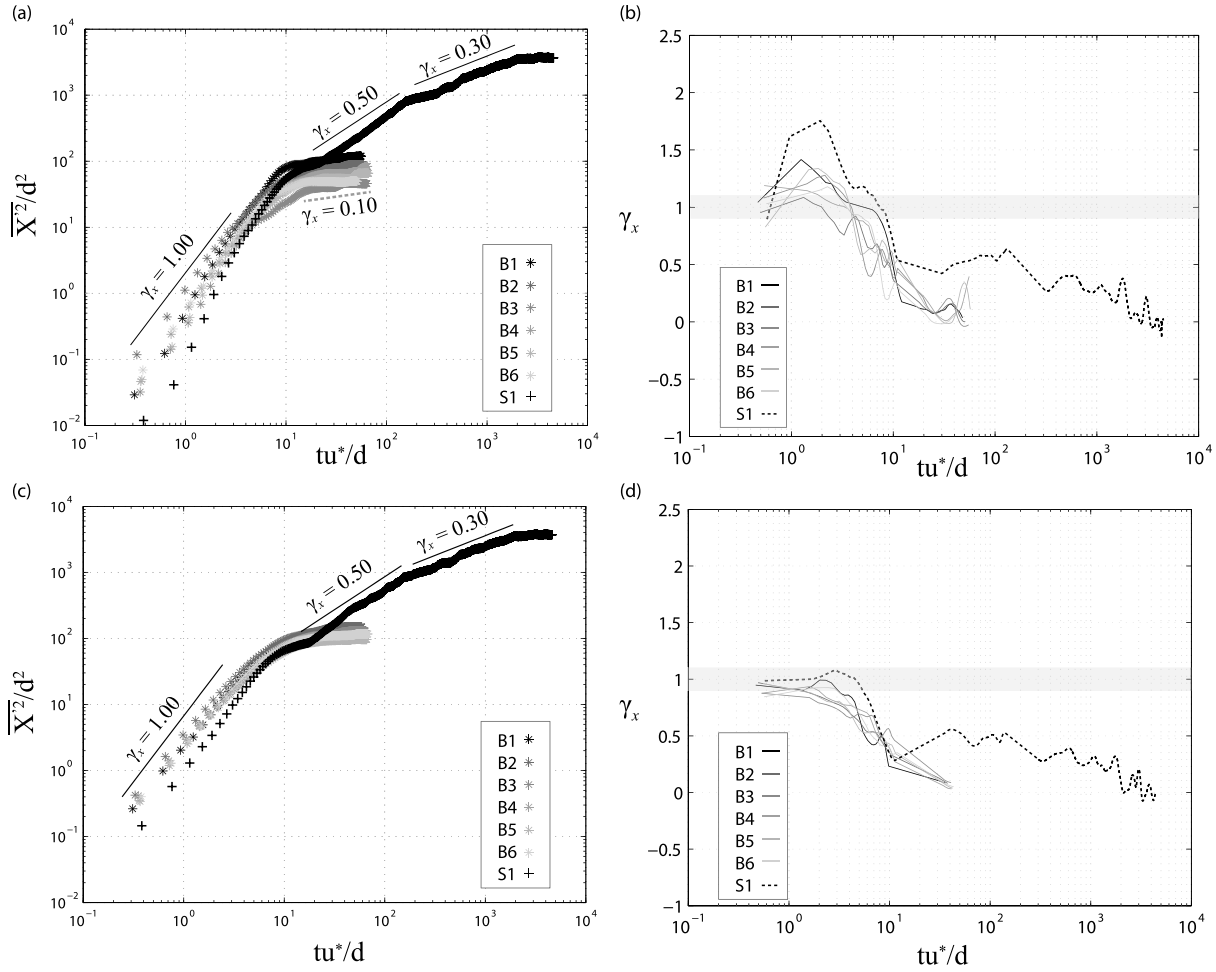

Figure 5. Temporal variation of $\overline{X'^2}/d^2$ and γ_x originating from entrainment points (a and b, respectively) and from randomly selected starting points (c and d, respectively).

found in this and previous studies, that is, $\gamma_x \approx 0.30$ (Nikora et al., 2002), although local values of γ_x fluctuate over a relatively wide range (Figure 5d). In this region data from B tests tend to underestimate γ_x, generating diffusive coefficients almost equal to zero (Figure 5c).

4.2. Transverse Diffusive Regimes

Compared to longitudinal diffusion from entrainment events, particle lateral coordinates exhibit a more irregular pattern identified by an initial smooth region with constant diffusive scaling coefficient, followed by a weaker subdiffusion regime (Figure 6a).

Clearer insight is given by closer inspection of the local variation of γ_y (Figure 6b) as the initial acceleration phase, characterized by superballistic diffusion in the streamwise direction ($\gamma_x > 1.0$), is now replaced by a ballistic regime (Campagnol et al., 2015). This ballistic regime has relatively short duration, spreading over the range $0.5 < tu^*/d < 1.5$. Closer observations of data from the annular flume reveal that the initial diffusive regime for S1and for the tests performed at weaker transport conditions (B1, B2, B3) is superdiffusive in the early stages of motion ($\gamma_y \approx 0.80$). After the short ballistic regime, γ_y decreases to a constant subdiffusive value that is maintained invariant for $tu^*/d > 10$. The change from ballistic to subdiffusive regime occurs gradually, and a smooth transition can be identified for $2 < tu^*/d < 10$, where $\overline{Y'^2}$ is no longer increasing with time with constant γ_y. For $tu^*/d > 10$, steady conditions are attained with scaling coefficient $\gamma_y = 0.20$, despite that broad fluctuations can still be observed around this average value as shown in Figure 6b.

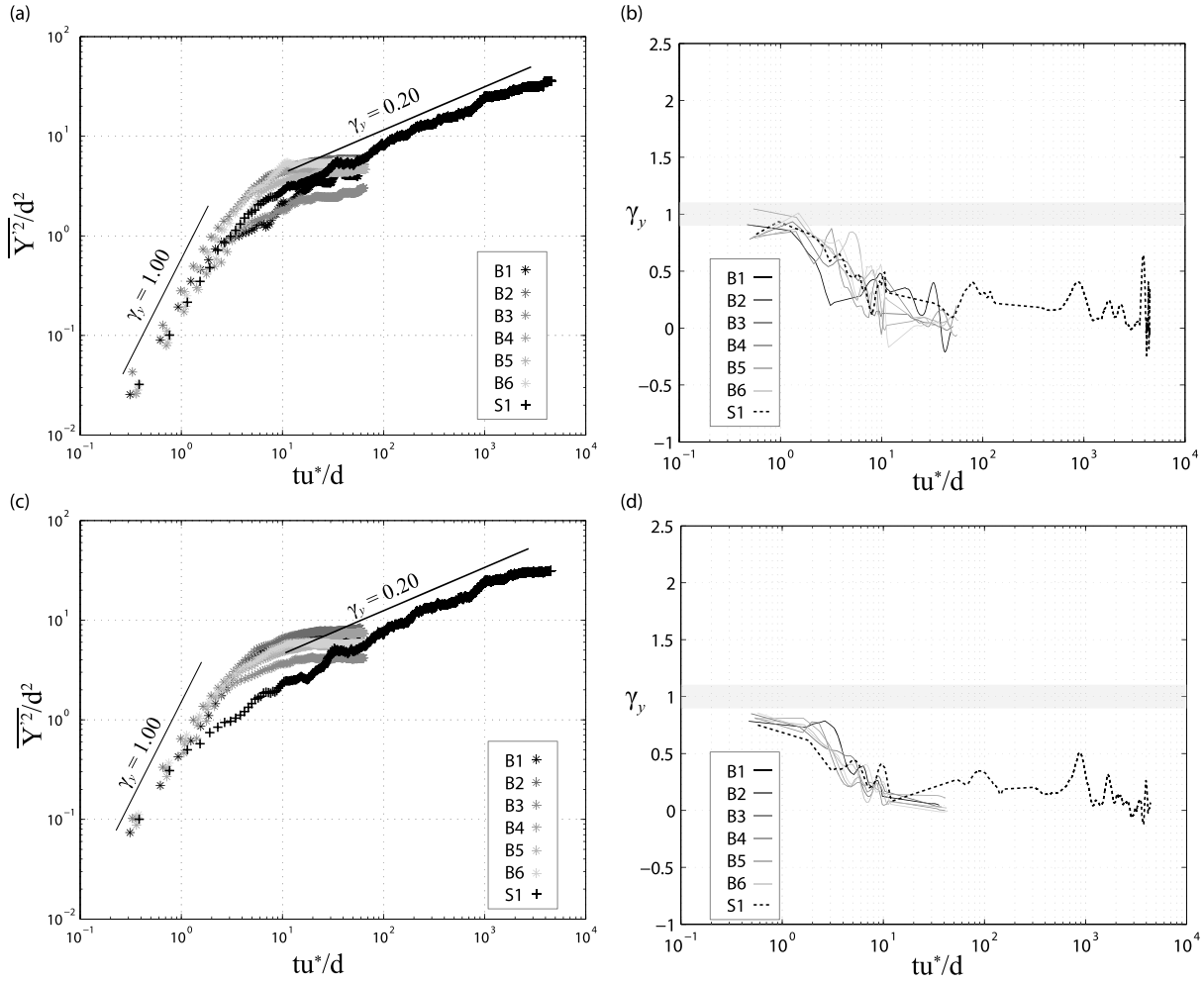

Figure 6. (a) Change in time of $\overline{Y'^2}$ and variation of γ_y for the case of entrainment starting points (a and b, respectively) and randomly selected starting points (c and d, respectively).

The character of diffusion was observed to vary if the starting point is moved to a location randomly selected along the particle displacements. When trajectories are referenced to an arbitrary coordinate identifying a *move* state, the initial regime becomes superdiffusive, with diffusive scaling coefficients γ_y = 0.70–0.80 (Figures 6c and 6d). Data from Test S1 exhibits the smallest scaling coefficient ($\gamma_y \approx 0.5$), as found for the entrainment-based approach. This early superdiffusive regime continues for $0.5 < tu^*/d < 1.5$, as observed for longitudinal diffusion. Afterward, a transition takes place where, regardless of relatively large fluctuations, the diffusive behavior reduces to attain steady conditions with constant scaling coefficient $\gamma_y = 0.20$, which confirms the presence of subdiffusion for longer time scales ($tu^*/d > 10$) along the transverse direction. As for longitudinal diffusion, for the B tests the interpretation of data may be misleading and the resulting diffusive scaling coefficient biased by censorship effects.

4.3. Effects of Experimental Censorship of Particle Trajectories

Recognition of the importance of the size of the detection window is recently new to the study of particle motion in laboratory experiments (Ballio et al., 2018; Bialik & Karpiński, 2018; Fan et al., 2017). The uncensored database collected with the annular flume was used to clarify to which extent results from B tests are to be considered reliable. By progressively reducing the longitudinal and transverse size of the observation area, trajectories extending beyond the simulated boundaries no longer contribute to the ensemble $\overline{X'^2}$. A decrease in the growth rate of the first and second order moments of particle locations is observed for B tests compared with results from uncensored data. Figures 7a and 7b show the effect of a reduced detection

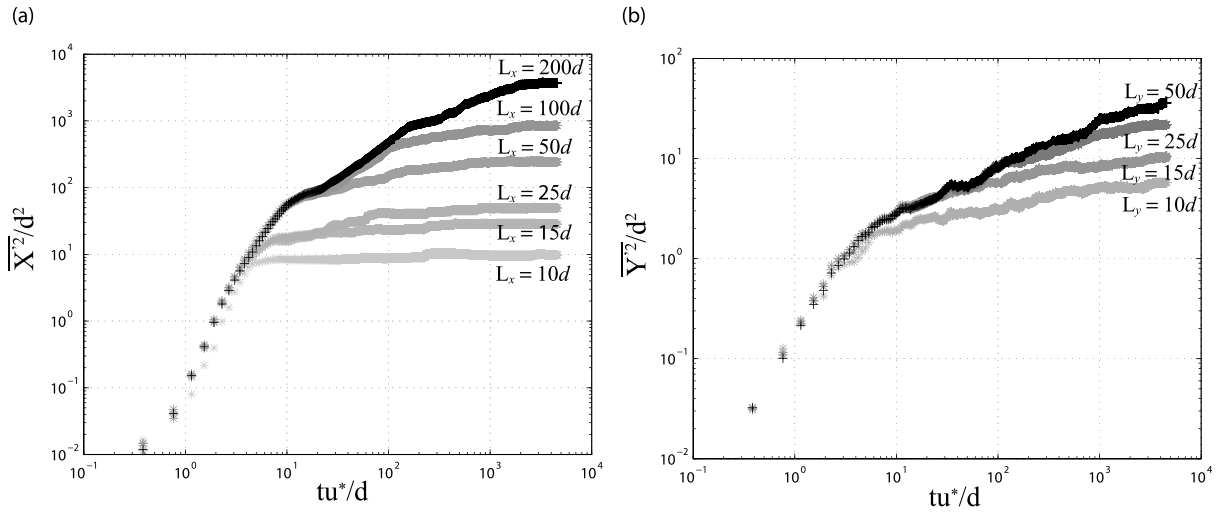

Figure 7. Results on (a) longitudinal and (b) transverse diffusion for different sizes of the investigated area. Test S1 from entrainment point.

window on the longitudinal and transverse diffusion, respectively, from entrainment points. For comparison with Bialik and Karpiński (2018), the longitudinal dimension $L_x = kd$ (with d the size of the moving particle) was reduced by applying scale factor k = 10, 15, 25, 50, 100, and 200 (corresponding to L_x ranging between 40 and 800 mm). The same scale factor was applied to the width L_y with k varying up to 50, which corresponds to the full channel width (200 mm). Decreasing k results in the portion of the plot that provides real diffusive trend to be significantly reduced, with an apparent departure for normalized time scales larger than the time scale corresponding to the initial motion of the particles ($tu^*/d > 3$). For the smallest detection windows (L_x = 10, L_y = 10), only the initial longitudinal superballistic and transverse ballistic regimes can still be observed, whereas the assessment of the later diffusive behavior is considerably biased, that is, for $tu^*/d > 3$. Censorship effects are less significant for diffusion in the transverse dimension, where data are consistent with the uncensored data up to $tu^*/d \approx 10$ for k = 15. This is argued to be dependent on the different extent that particles travel along the two directions, respectively. As particles mainly move downstream, the distance they travel in the lateral direction is limited to a few grain diameters, with hiding effects due to the local bed geometry created by the surrounding particles being more significant than in the streamwise direction.

The observation area used in the B tests (220 by 80 mm) is close to the case $L_x = 50d$ and $L_y = 15d$.It is expected that the portion of the plot that is censorship-free extends for up to $tu^*/d \approx 3$ (slightly further for transverse diffusion), as also apparent from Figures 5a and 6a.

5. Discussion: Temporal and Spatial Scales of Diffusive Regimes

The analysis of bed load particle diffusion performed from different starting coordinates (entrainment and random motion) demonstrated the existence of two distinct diffusive behaviors, composed by diffusive regimes affecting longitudinal and transverse trajectories that can be identified with constant scaling coefficients and well-defined time scales. Evidence of these behaviors is graphically summarized in Figure 8, which critically revise the conceptual model presented in Figure 1.

5.1. Local Range

The first regime, corresponding to continuous particle motion between collisions with the bed, is superdiffusive with $\gamma_x\gamma_y > 0.50$, and the initiation of movement when particles are subject to acceleration takes place for $tu^*/d \leq 3$. This is in agreement with the threshold found by Bialik et al. (2015) through the application of a turbulent structures generator that discriminated between the near-field and ballistic subranges (Bialik, 2013), and close to the threshold observed by Campagnol et al. (2015), tu^*/d = 1.5–2.5. Within this region the longitudinal diffusive scaling coefficient indicates a superballistic regime, $1.0 < \gamma_x < 2.0$, with exponents dependent on transport conditions and bed material. Under weak transport conditions the superballistic

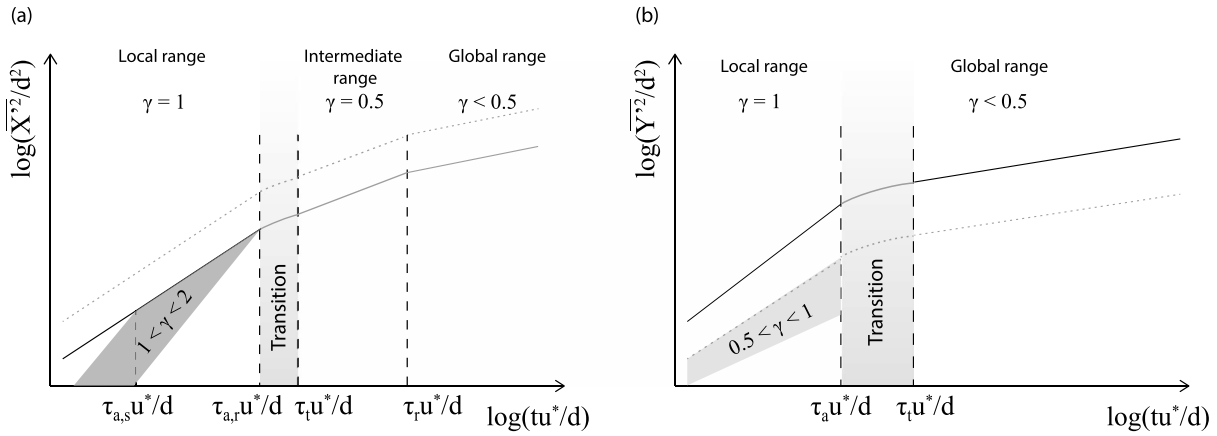

Figure 8. Revised diffusive regimes for longitudinal (a) and transverse (b) displacements (after Nikora et al., 2002 and Campagnol et al., 2015). Dotted gray lines represent diffusion from randomly selected points, continuous lines diffusion from entrainment points. Characteristic times $\tau_{a,s}$ and $\tau_{a,r}$ indicate the duration of the acceleration for saltating and rolling particles, respectively, while τ_t indicates the mean travel time and τ_r the resting time of moving particles.

regime lasts over a longer period, with dimensionless times up to $tu^*/d = 4$ to 5, due to a longer acceleration phase of particles mainly rolling over the bed. As in these transport conditions the acceleration phase governs a larger portion of the initial trajectory (Bialik et al., 2015; Campagnol et al., 2015), the local range is likely to account for values of $\gamma_x > 1.0$. This is confirmed by direct inspection of data from test B1, which was performed under comparable weak transport conditions as for test S1. The local values of γ_x for this test are the highest among the other companion tests, and its variation with time closely resembles the data trend obtained for test S1.

The role played by bed material is apparent from observing the magnitude of γ_x, with larger values of the scaling coefficient for a bed made of spheres ($\gamma_x \approx 2.0$) than in the case of natural gravel ($1.0 < \gamma_x < 1.5$). Since data from the B tests were obtained for bed load gravel moving over a natural bed, at entrainment, particles might not experience a significant acceleration, due to the different interaction with the roughness created by the surrounding gravel material during the initial collisions with the bed. By contrast, in an artificial bed made of spheres, the mechanics of particle entrainment for a geometrically packed, well-organized bed material is likely to cause a rapid acceleration phase. This explains the higher values of γ_x found for test S1, which is typical of a group of particles accelerating along the streamwise direction (Campagnol et al., 2015), as suggested by Bialik et al. (2015) in their numerical study on diffusive behavior for spheres.

Although data from Test S1 (spheres in annular flume) suggest that spheres are rapidly accelerated into motion (Campagnol et al., 2015), values of γ_x reported in this study are lower than those presented by Bialik et al. (2012) for the entrainment of fully exposed spherical particles. It is argued that the counteracting mechanisms of the packing arrangement of bed material (frictional forces) and the protrusion of mobile particles over the surrounding bed elements (exposure to fluid drag) significantly contribute to the development of superballistic behavior.

Once a particle is brought into motion and attains steady velocity, diffusion is dominated by inertia, with particles moving in a dynamic balance between fluid forces, submerged weight, and bed heterogeneities (Bialik et al., 2015; Martin et al., 2012; Nikora et al., 2002). Ballistic diffusion is observed to occur when considering a randomly selected coordinate along the grain path as the starting point. In this case the acceleration phase (superballistic diffusion) does not significantly contribute, as the population sample largely included trajectories from points within a steady state of motion (Campagnol et al., 2015). The superballistic regime is completely replaced by ballistic diffusion in the local range ($tu^*/d \leq 3$), confirming the conceptual model of Nikora et al. (2002) and following formulations proposed by Campagnol et al. (2015).

Heterogeneity of local grain arrangements and bed roughness significantly affect diffusion processes along the transverse direction with near-bed flow turbulence being a minor factor in the dynamics of particle diffusion (Bialik et al., 2012). Lateral motion is more erratic (Furbish, Ball, & Schmeeckle, 2012) and in its early stage, particles do not experience significant acceleration, presenting ballistic diffusion for $0.5 < tu^*/d < 1.5$. This is

ascribed to the dominant role of frictional forces on transverse diffusion, as the instantaneous drag exerted by the fluid in the lateral direction is smaller by at least 1 order of magnitude than the forces experienced by individual particles in the streamwise direction (Furbish, Ball, & Schmeeckle, 2012). Unexpectedly, this analysis also shows that gravel experiences larger accelerations than spheres in the lateral direction, thus exhibiting opposite behavior compared to findings reported for the longitudinal acceleration. It is argued that in an artificial bed arrangement created by regular spheres, lift due to the Bernoulli pressure difference plays a major role (compared to the lateral drag) in dislodging particles that are mainly entrained into motion with upward acceleration (e.g., Detert et al., 2010; Dwivedi et al., 2011). With the random-point approach superdiffusion ($0.5 < \gamma_y < 1$) is found to occur for $tu^*/d < 3$ as reported by Furbish, Ball, and Schmeeckle (2012), which proves that the effect of bed heterogeneity on the erratic nature of lateral motion is important for already moving particles.

No clear evidence was found on the effects of the applied shear stress on the diffusion process, except for the two tests performed under weak transport conditions (tests S1 and B1). For all the other tests, variation in shear velocity was not observed to affect the diffusion regime suggesting that in the early stage of motion turbulence (and bed roughness for diffusion in the lateral direction) plays a dominant role, while for well-developed trajectories inertia and interactions with the bed mostly control the diffusive behavior of particle motion.

5.2. Intermediate Range

The intermediate range associated to normal diffusion is supported by experimental evidence gained from the experiment S1, while no definitive conclusions can be drawn for data collected from the B tests due to censorship effects reported in section 4.3. A regime of reasonably steady normal diffusion along the longitudinal direction starts developing approximately for $tu^*/d \approx 10$, close to the threshold between superdiffusive and subdiffusive regimes as identified by Nikora et al. (2002), who obtained $tu^*/d = 15$ from their analysis. In the earlier transitional region, that is, $3 < tu^*/d < 10$, the longitudinal scaling coefficient was observed to decrease from superballistic (or ballistic if random point analysis is applied) to Fickian values, partially in contrast with findings presented by Nikora et al. (2002). They postulated the existence of a steady superdiffusive regime in the region from $tu^*/d = 0.2$ to 7–8, that is, within a temporal window that might have partly incorporated the diffusive (ballistic) process occurring in the local range, thus originating a superdiffusive regime with constant scaling coefficient $\gamma < 1.0$. Similar conclusions can be found in the numerical work of Bialik et al. (2015), who attributed such discrepancies to the mixing of bordering diffusive regimes from local and global ranges. However, the hypothesis that in the intermediate range diffusion may be either slow ($\gamma < 0.5$), normal ($\gamma \approx 0.5$), or super ($\gamma > 0.5$), was indeed originally predicted by Nikora et al. (2002), arguing that this is dependent on what factors dominate. Bed topography, which is inherently correlated to intermittent motion for weak transport stages, and near-bed turbulence may have opposite effects, with the former inducing slow diffusion processes ($\gamma < 0.5$), while turbulence may enhance them ($\gamma > 0.5$), or they can potentially mutually cancel their effects ($\gamma \approx 0.5$). This latter case is apparently the most representative of the specific experimental conditions tested in our study.

After the acceleration phase, trajectories are found to be mostly affected by particle dynamics, as inertia and bed heterogeneity prevail for times smaller than particle traveling times, thus resulting in the observed superdiffusion of the transitional region (Martin et al., 2012). In this study the mean traveling time (time from entrainment to rest) is $\tau_t = 0.90$ s for test S1 (annular flume). If normalized with the characteristic time u^*/d, this value corresponds to the beginning of the region where normal diffusion occurs for S series of data, that is, for $tu^*/d \approx 10$. As the observation time approaches the mean particle traveling time, diffusion is likely to preserve those mechanical aspects defining the continuous motion in the local range, resulting in superdiffusion (transitional region). For longer observation periods, some particles will stop in a rest state, so that the resting times increasingly contribute to the diffusion process, and the ensemble spreading of the plume grows linearly with time until $tu^*/d \approx 100$. After this time scale (which is anticipated to correspond to the mean resting time of the moving grains) rest periods become a key factor in driving a new diffusive process. Under these intermediate conditions normal diffusion is thus argued to arise from balancing the effects due to near-bed turbulence and slowly intermittent but continuous particle motion, with resting times reasonably following probability distributions having finite variance, for example, exhibiting exponential-like behaviors. For larger times this assumption may no longer hold if bed-mixing processes become dominant and resting

times potentially achieve nonfinite values leading to heavy-tailed distribution. This can be reasonably expected when trapping processes are favored by the low stages of sediment transport, thus significantly counteracting the super-diffusive effects of near-bed turbulence.

A wider range of grain sizes may result in different diffusive regimes, since the mixed bed material would enhance hiding and exposure effects, thus considerably affecting individual grain displacements (Ferguson et al., 2002; Ganti et al., 2010).

The transitional region is observed also along the lateral direction, starting at the end of the superdiffusive regime and developing for up to the time scale corresponding to the particle mean resting time, that is, $2 < tu^*/d < 10$. This transition is found to last longer for transverse motion possibly due to the more erratic behavior of particle displacements in the lateral direction. The diffusive behavior thus differs compared to the longitudinal diffusion as it evolves in a subdiffusive regime that is approximated by a constant scaling coefficient $\gamma_y = 0.20$. As for the transverse component of transport, frictional forces are comparable to the instantaneous lateral drag (for tests B, $u^* \approx$ 70-80 mm/s, maximum lateral velocity fluctuations $\approx \pm$50 mm/s), $\overline{Y'^2}$ is found to increase in time at lower rates compared to diffusion along the longitudinal direction, resulting in anisotropic subdiffusive behavior.

5.3. Global Range

As argued by Fan et al. (2017), areal limitations, particularly along the longitudinal direction, affect the proper assessment of the variance of particle locations. The global range consists of time periods when particles are in motion alternated by rest periods. Proper consideration of diffusive processes in the global range requires long enough records of particle motion, that is, longer than the mean traveling and resting times, which means the image acquisition system and the size of the investigation area must enable observation of several entrainment and distrainment events for each tracked particle. For the tests carried out in the straight flume the mean resting time of particles that moved at least once ranged between $\tau_r = 4$ and 5 s, resulting in an average $\tau_r u^*/d = 65$, which is close to the largest dimensionless time explored. The reported mean resting time is likely affected by data censorship (Ballio et al., 2018). It can be argued that the investigated area in the straight flume was too short to enable direct observation of global ranges. For the test carried out in the annular flume particles, positions were recorded for time periods well beyond the mean resting time of the moving particles ($\tau_r = 11.4$ s, that is $\tau_r u^*/d = 130$), thus ensuring repeated observations of global trajectories. However, it is remarked that, despite experimental data from the annular flume fall within the global range according to the criteria suggested by Bialik and Karpiński (2018), the latter could possibly not be definitively assessed in this study due to temporal (rather than spatial) censorship effects. This is particularly true in light of the evidence that resting times possibly exhibit a bimodal-like behavior (see discussion in the next paragraph), which accounts for extremely long periods of rest that extend well beyond the observation time window of our experiment

The third regime (or second in the case of transverse motion) denoted by constant scaling coefficient confirms that bed load particles subdiffusivity occurs at longer times. Diffusion in the global range is found to be anisotropic with $\gamma_x = 0.30$ (longitudinal diffusion) and $\gamma_y = 0.20$ (lateral diffusion), in agreement with findings of Nikora et al. (2002). Anomalous diffusion (subdiffusion) is expected in the global range as the statistical distribution of particle resting times becomes increasingly central in driving the process (Bialik et al., 2015; Martin et al., 2012; Nikora et al., 2002). Subdiffusion originates from heavy-tailed distributions of resting times (Bradley, 2017) as reentrainment is a result of the dynamic balance between instantaneous drag forces and local bed scouring (Martin et al., 2012). The latter is responsible for longer states of rest as buried particles were sheltered from exposure to the fluid, while vertical mixing of surface and subsurface material was observed to increase with time (Hassan & Church, 1994; Marion & Fraccarollo, 1997) and with the intensity of the competent flow (Wong et al., 2007). Even if the distributions of resting times are affected by experimental censorship (corresponding to the end of the observation time), the annular flume enabled measuring resting times over significantly long observation periods. Resting times were calculated for tracers that moved at least once and consisted of measurable resting periods for which the reentrainment event was observed before the end of the recording subsession. For grains found at rest at the end of each subsession, resting times could not be estimated accurately as $t_{end} < t_{re\text{-}entr}$, with t_{end} the total duration of the observation period and $t_{re\text{-}entr}$ the instant of the subsequent reentrainment event. Their extreme values are limited in

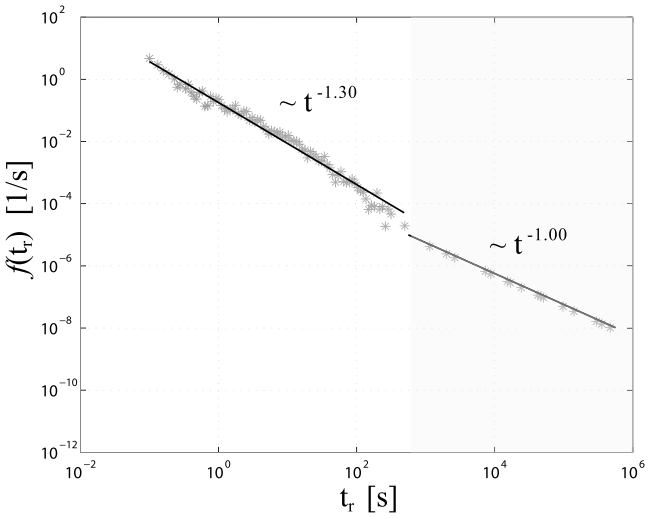

Figure 9. Distribution of the resting times for test S1. The gray area indicates the population of longer resting times.

number, representing on average 8% of the population sample; however, they would produce heavier-tailed distributions causing an increase of statistical parameters. By monitoring the positions of this small group of particles over the 6-hr duration of the experiment along the area observed by the six cameras, their waiting times were found to be on average 3,000 s with standard deviation 4,800 s. The complete population of rest times characterized by smaller statistics (i.e., mean τ_r = 11.4 s) and the subset including extreme waiting times (i.e., mean $\tau_r \approx$ 3,000 s) are argued to identify two different rest mechanisms, respectively, with the former associated with the continuous motion of particles, the latter with vertical mixing. If combined together, the two population samples provide mean resting time of about 800 s with heavy-tailed frequency distribution, approaching zero more slowly than an exponential distribution (Figure 9).

However, data reported from the experiment in the annular flume include measurements up to tu^*/d = 4,600 (corresponding to t = 400 s), which is significantly lower than the average resting time of the second subset of particles (exhibiting long-standing resting times), so that the vertical mixing effect on the global regime cannot be fully accounted for in this study.

6. Conclusions

A detailed analysis of diffusive regimes at different stages of bed load transport has been carried out using novel experimental data obtained from observations of sediment tracers in annular flume. The original conceptual model proposed by Nikora et al. (2002), and subsequently modified by Campagnol et al. (2015), has been critically revised to account for different starting points of particle trajectories and to link well-defined time scales to the diffusion of bed load sediment.

The local range is governed by inertia and local bed heterogeneities, resulting in longitudinal ballistic (γ_x = 1.0) and lateral superdiffusive regimes ($0.5 < \gamma_y < 1.0$), respectively, while acceleration from entrainment is the key mechanism driving longitudinal superballistic ($1.0 < \gamma_x < 2.0$) and lateral ballistic regimes (γ_y = 1.0) during the early accelerating stage of motion. The dimensionless acceleration time associated with entrainment events is in agreement with previous findings of Bialik et al. (2015) and Campagnol et al. (2015), that is, $\tau_{a,x}u^*/d \approx 3$ and $\tau_{a,y}u^*/d$ = 1.0–2.0, with τ_a the duration of acceleration along the selected direction.

For $t > \tau_t$ (= mean traveling time), inertial effects are slowly replaced by mechanisms controlling particle resting times, leading to normal diffusive transport (γ_x = 0.5) in the intermediate range. As originally predicted by Nikora et al. (2002), this is first experimentally confirmed to be the result of counteracting effects due to intermittent weak transport conditions and near-bed turbulence. For times longer than the mean particle resting period, that is, ($t > \tau_r$), the motionless state of a significant fraction of particles becomes the key parameter in driving the diffusion process. The physical processes controlling the distribution of resting times, which were observed to be heavy tailed and dependent on the vertical mixing of surface and subsurface material, are responsible for subdiffusion for $t > \tau_r$. Such anomalous diffusion is expected to arise when the Central Limit Theorem does not hold, as broad distributions exist with diverging first or second moments of particle motion.

Due to the short distance traveled by the particles in the lateral direction, diffusion is found to be clearly anisotropic with γ_x = 0.30 and γ_y = 0.20.The analysis demonstrated the effects of experimental censorship on the proper identification of diffusive regimes, due to the fixed boundaries of the investigation area and to the temporal duration of the observations. The assigned lateral dimension is shown to play a minor role, while the longitudinal dimension greatly influences the accurate estimation of the diffusion coefficients in the intermediate and global ranges. Censored data could then compromise the validity of results about diffusive behavior of bed load particles.

Although the present experimental results are limited to uniformly sized bed material, they have significant implications for stochastic transport models that aim to predict the fate of a sediment plume (from entrainment of grains) or flux (from randomly selected points), as they shade new light on the nature of the diffusive

process at different stages of bed load motion. Even if the observed diffusive behavior is expected to find validity also in natural rivers, a broader understanding of the physical processes governing diffusion should consider the influence of sediment mixtures typical of natural streams, where hiding and exposure factors might play a role in determining the diffusive character at different stages of transport.

Acknowledgments
This work was supported by the Research Executive Agency, through the 7th Framework Programme of the European Union, Support for Training and Career Development of Researchers (Marie Curie-FP7-PEOPLE-2012-ITN), which funded Initial Training Network (ITN) HYTECH "Hydrodynamic Transport in Ecologically Critical Heterogeneous Interfaces," N. 316546.The data used are listed in the references and tables.

References

Abbott, J. E., & Francis, J. R. D. (1977). Saltating and suspended trajectories of solid grains in a water stream. *Philosophical Transactions of the Royal Society London A*, *284*(22), 5254.

Ballio, F., Pokrajac, D., Radice, A., & Hosseini Sadabadi, S. A. (2018). Lagrangian and Eulerian description of bed load transport. *Journal of Geophysical Research: Earth Surface*, *123*, 384–408. https://doi.org/10.1002/2016JF004087

Bialik, R. J. (2013). Numerical study of near-bed turbulence structures influence on the initiation of saltating grains movement. *Journal of Hydrology and Hydromechanics*, *61*(3), 202–207. https://doi.org/10.2478/johh-2013-0026

Bialik, R. J., & Karpiński, M. (2018). On the effect of the window size on the assessment of particle diffusion. *Journal of Hydraulic Research*, *56*(4), 560–566. https://doi.org/10.1080/00221686.2017.1397780

Bialik, R. J., Nikora, V. I., Karpiński, M., & Rowinski, P. M. (2015). Diffusion of bedload particles in open-channel flows: Distribution of travel times and second-order statistics of particle trajectories. *Environmental Fluid Mechanics*, *15*(6), 1281–1292. https://doi.org/10.1007/s10652-015-9420-5

Bialik, R. J., Nikora, V. I., & Rowinski, P. M. (2012). 3D lagrangian modelling of saltating particles diffusion in turbulent water flow. *Acta Geophysica*, *60*(6), 1639–1660. https://doi.org/10.2478/s11600-012-0003-2

Booij, R. (1994). Measurements of the flow field in a rotating annular flume. In *Communications on hydraulic and geotechnical engineering*, (Rep. No 94–92, 58 pp.). Delft, The Netherlands: Delft University of Technology.

Bottacin-Busolin, A., Tait, S. J., Marion, A., Chegini, A., & Tregnaghi, M. (2008). Probabilistic description of grain resistance from simultaneous flow field and grain motion measurements. *Water Resources Research*, *44*, W09419. https://doi.org/10.1029/2007WR006224

Bouchaud, J., & Georges, A. (1990). Anomalous diffusion in disordered media: Statistical mechanisms, models and physical applications. *Physics Reports*, *195*(4-5), 127–293. https://doi.org/10.1016/0370-1573(90)90099-N

Bradley, D. N. (2017). Direct observation of heavy-tailed storage times of bed load tracer particles causing anomalous superdiffusion. *Geophysical Research Letters*, *44*, 12,227–12,235. https://doi.org/10.1002/2017GL075045

Bradley, D. N., Tucker, G. E., & Benson, D. A. (2010). Fractional dispersion in a sand bed river. *Journal of Geophysical Research*, *115*, F00A01. https://doi.org/10.1029/2010JF001661

Campagnol, J., Radice, A., Ballio, F., & Nikora, V. I. (2015). Particle motion and diffusion at weak bed load: Accounting for unsteadiness effects of entrainment and disentrainment. *Journal of Hydralics Research*, *53*(5), 633–648. https://doi.org/10.1080/00221686.2015.1085920

Campagnol, J., Radice, A., Nokes, R., Bulankina, V., Lescova, A., & Ballio, F. (2013). Lagrangian analysis of bed-load sediment motion: Database contribution. *Journal of Hydraulic Research*, *51*(5), 589–596. https://doi.org/10.1080/00221686.2013.812152

Cecchetto, M., Tregnaghi, M., Bottacin-Busolin, A., Tait, S., & Marion, A. (2016). Statistical description on the role of turbulence and grain interference on particle entrainment from gravel beds. *Journal of Hydraulic Engineering*, *143*(1). https://doi.org/10.1061/(ASCE)HY.1943-7900.0001224

Detert, M., Weitbrecht, V., & Jirka, G. H. (2010). Laboratory measurements on turbulent pressure fluctuations in and above gravel beds. *Journal of Hydraulic Engineering*, https://doi.org/10.1061/(ASCE)HY.1943-7900.0000251, *136*(10), 779–789.

Dey, S., Sarkar, S., & Solari, L. (2011). Near-bed turbulence characteristics at the entrainment threshold of sediment beds. *Journal of Hydraulic Engineering*,https://doi.org/10.1061/(ASCE)HY.1943-7900.0000396, *137*(9), 945–958.

Drake, T. G., Shreve, R. L., Dietrich, W. E., Whiting, P., & Leopold, L. B. (1987). Bed load transport of fine gravel observed by motion-picture photography. *Journal of Fluid Mechanics*, *192*, 193–217.

Dwivedi, A., Melville, B., Shamseldin, A. Y., & Guha, T. K. (2011). Analysis of hydrodynamic lift on a bed sediment particle. *Journal of Geophysical Research*, *116*, F02015. https://doi.org/10.1029/2009JF001584

Fan, N., Xie, Y., & Nie, R. (2017). Bed load transport for a mixture of particle sizes: Downstream sorting rather than anomalous diffusion. *Journal of Hydrology*, *553*, 26–34. https://doi.org/10.1016/j.jhydrol.2017.07.012

Fathel, S. L., Furbish, D. J., & Schmeeckle, M. W. (2015). Experimental evidence of statistical ensemble behavior in bed load sediment transport. *Journal of Geophysical Research: Earth Surface*, *120*, 2298–2317. https://doi.org/10.1002/2015JF003552

Ferguson, R. I., Bloomer, D. J., Hoey, T. B., & Werritty, A. (2002). Mobility of river tracer pebbles over different timescales. *Water Resources Research*, *38*(5), 1045. https://doi.org/10.1029/2001WR000254

Ferguson, R. I., & Hoey, T. B. (2002). Long-term slowdown of river tracer pebbles: Generic models and implications for interpreting short-term tracer studies. *Water Resources Research*, *38*(8), 1142. https://doi.org/10.1029/2001WR000637

Ferguson, R. I., & Wathen, S. J. (1998). Tracer-pebble movement along a concave river profile: Virtual velocity in relation to grain size and shear stress. *Water Resources Research*, *34*, 2031–2038. https://doi.org/10.1029/98WR01283

Furbish, D. J., Ball, A. E., & Schmeeckle, M. W. (2012). A probabilistic description of the bed load sediment flux: 4. Fickian diffusion at low transport rates. *Journal of Geophysical Research*, *117*, F03034. https://doi.org/10.1029/2012JF002356

Furbish, D. J., Roseberry, J. C., & Schmeeckle, M. W. (2012). A probabilistic description of the bed load sediment flux: 3. The particle velocity distribution and the diffusive flux. *Journal of Geophysical Research*, *117*, F03033. https://doi.org/10.1029/2012JF002355

Ganti, V., Meerschaert, M. M., Foufoula-Georgiou, E., Viparelli, E., & Parker, G. (2010). Normal and anomalous diffusion of gravel tracer particles in rivers. *Journal of Geophysical Research*, *115*, F00A12. https://doi.org/10.1029/2008JF001222

Gharabaghi, B., Inkratas, C., Krishnappan, B. G., & Rudra, R. P. (2007). Flow characteristics in a rotating circular flume. *The Open Civil Engineering Journal*, *1*(1), 30–36. https://doi.org/10.2174/1874149500701010030

Grass, A. J. (1970). Initial instability of fine sand. *Journal of the Hydraulics Division*, *96*(3), 619–632.

Haschenburger, J. K. (2011). Vertical mixing of gravel over a long flood series. *Earth Surface Processes and Landforms*, *36*(8), 1044–1058. https://doi.org/10.1002/esp.2130

Hassan, M. A., & Church, M. (1994). Vertical mixing of coarse particles in gravel bed rivers: A kinematic approach. *Water Resources Research*, *30*, 1173–1185. https://doi.org/10.1029/93WR03351

Hassan, M. A., Church, M., & Ashworth, P. J. (1992). Virtual rate and mean distance of travel of individual clasts in gravel-bed channels. *Earth Surface Processes and Landforms*, *17*(6), 617–627. https://doi.org/10.1002/esp.3290170607

Hassan, M. A., Voepel, H., Schumer, R., Parker, G., & Fraccarollo, L. (2013). Displacement characteristics of coarse fluvial bed sediment. *Journal of Geophysical Research: Earth Surface*, *118*, 155–165. https://doi.org/10.1029/2012JF002374

Heays, K. G., Friedrich, H., Melville, B. W., & M.ASCE, and Nokes, R. (2014). Quantifying the dynamic evolution of graded gravel beds using particle tracking velocimetry. *Journal of Hydraulic Engineering*, *140*(7). https://doi.org/10.1061/(ASCE)HY.1943-7900.0000850

Hurley, R., Woodward, J., & Rothwell, J. J. (2018). Microplastic contamination of river beds significantly reduced by catchment-wide flooding. *Nature Geoscience*, *11*(4), 251–257. https://doi.org/10.1038/s41561-018-0080-1

James, P. W., Jones, T. E. R., & Stewart, D. M. (1996). Numerical and experimental studies of annular flume flow. *Applied Mathematical Modelling*, *20*, 225–231. https://doi.org/10.1016/0307-904X(95)00149-E

Lajeunesse, E., Devauchelle, O., Houssais, M., & Seizilles, G. (2013). Tracer dispersion in bedload transport. *Advances in Geosciences*, *37*, 1–6. https://doi.org/10.5194/adgeo-37-1-2013

Lajeunesse, E., Malverti, L., & Charru, F. (2010). Bed load transport in turbulent flow at the grain scale: Experiments and modeling. *Journal of Geophysical Research*, *115*, F04001. https://doi.org/10.1029/2009JF001628

Marion, A., & Fraccarollo, L. (1997). Experimental investigation of mobile armouring development. *Water Resources Research*, *33*, 1447–1453. https://doi.org/10.1029/97WR00705

Marion, A., Nikora, V., Puijalon, S., Bouma, T., Koll, K., Ballio, F., et al. (2014). Hydrodynamics and ecology: The critical role of interfaces in biophysical interaction. *Journal of Hydraulic Research*, *52*(6), 744–758. https://doi.org/10.1080/00221686.2014.968887

Martin, R. L., Jerolmack, D. J., & Schumer, R. (2012). The physical basis for anomalous diffusion in bed load transport. *Journal of Geophysical Research*, *117*, F01018. https://doi.org/10.1029/2011JF002075

Nathan Bradley, D., & Tucker, G. (2012). Measuring gravel transport and dispersion in a mountain river using passive radio tracers. *Earth Surface Processes and Landforms*, *37*, 1034–1045. https://doi.org/10.1002/esp.3223

Nelson, J. M., Shreve, R. L., Mclean, S. R., & Drake, T. G. (1995). Role of near-bed turbulence structure in bed load transport and bed form mechanics. *Water Resources Research*, *31*, 2071–2086. https://doi.org/10.1029/95WR00976

Nezu, I., & Nakagawa, H. (1993). Turbulence in Open-Channel Flows, Balkema, Rotterdam, Netherlands.

Nikora, V., & Goring, D. (2000). Flow turbulence over fixed and weakly mobile gravel beds. *Journal of Hydraulic Engineering*, https://doi.org/10.1061/(ASCE)0733-9429(2000)126:9(679), *126*(9), 679–690.

Nikora, V., Goring, D. G., McEwan, I., & Griffiths, G. (2001). Spatially averaged open-channel flow over rough bed. *Journal of Hydraulic Engineering*, *127*(2), 123–133. https://doi.org/10.1061/(ASCE)0733-9429(2001)127:2(123)

Nikora, V., Habersack, H., Huber, T., & McEwan, I. (2002). On bed particle diffusion in gravel bed flows under weak bed load transport. *Water Resources Research*, *38*(6), 1081. https://doi.org/10.1029/2001WR000513

Nino, Y., & Garcia, M. H. (1996). Experiments on particle turbulence interactions in the near wall regions of an open channel flow: Implications for sediment transport. *Journal of Fluid Mechanics*, *326*(1), 285–319. https://doi.org/10.1017/S0022112096008324

Paintal, A. S. (1969), The probabilistic characteristics of bed load transport in alluvial channels. *PhD dissertion*, University of Minnesota. Minneapolis, Minnesota, USA.

Partheniades, E., Kennedy, J. F., Etter, R. J., and Hayer, R. P. (1966), Investigations of the depositional behavior of fine cohesive sediments in annular rotating channel. *Rep. no 96*, Ralph M. Parsons, Hydrodynamics Laboratory, Massachusetts Institute of Technology, Cambridge, Massachusetts, USA.

Roseberry, J. C., Schmeeckle, M. W., & Furbish, D. J. (2012). A probabilistic description of the bed load sediment flux: 2. Particle activity and motions. *Journal of Geophysical Research*, *117*, F03032. https://doi.org/10.1029/2012JF002353

Schmeeckle, M. W., & Nelson, J. M. (2003). Direct numerical simulation of bedload transport using a local, dynamic boundary condition. *Sedimentology*, *50*, 279–301. https://doi.org/10.1046/j.1365-3091.2003.00555.x

Tregnaghi, M., Bottacin-Busolin, A., Marion, A., & Tait, S. (2012). Stochastic determination of entrainment risk in uniformly sized sediment beds at low transport stages: 1. Theory. *Journal of Geophysical Research*, *117*, F04004. https://doi.org/10.1029/2011JF002134

Tregnaghi, M., Bottacin-Busolin, A., Tait, S., & Marion, A. (2012). Stochastic determination of entrainment risk in uniformly sized sediment beds at low transport stages: 2. Experiments. *Journal of Geophysical Research*, *117*, F04005. https://doi.org/10.1029/2011JF002134

van Rijn, L. (1984). Sediment pick-up function. *Journal of Hydraulic Engineering*, *110*(10). https://doi.org/10.1061/(ASCE)0733-9429(1984)110:10(1494)

Vanoni, V. (1975), Sedimentation engineering. *ASCE Manual* n.54.

Wong, M., Parker, G., DeVries, P., Brown, T. M., & Burges, S. J. (2007). Experiments on dispersion of tracer stones under lower-regime plane-bed equilibrium bed load transport. *Water Resources Research*, *43*, W03440. https://doi.org/10.1029/2006WR005172

Yalin, M. S. (1972). *Mechanics of sediment transport*. Oxford, New York: Pergamon Press.